

HIGH EFFICIENT VISIBLE-LIGHT ACTIVATED PHOTO CATALYTIC SEMICONDUCTOR SnO₂/Sn₃O₄ HETEROSTRUCTURE IN DIRECT BLUE 71 (DB71) DEGRADATION

Adri Huda¹, I Putu Mahendra², Reisyah Ichwani³, Chanel Tri Handoko¹,
Ha Minh Ngoc⁴, Bambang Yudono¹, Muhammad Djoni Bustan^{1*},
and Fakhili Gulo^{1*}

¹Program Studi Doktor Ilmu Lingkungan, Program Pascasarjana-Universitas Sriwijaya,
Palembang-30139, Indonesia

²Departemen Kimia, Fakultas Matematika dan Ilmu Pengetahuan Alam-Universitas Sumatera
Utara, Medan-20155, Indonesia

³Department of Material Science and Engineering, Worcester Polytechnic Institute,
Worcester-MA-01609, United States

⁴Key Laboratory of Advanced Material for Green Growth, Vietnam National University, Hanoi
University of Science, Hanoi-100000, Viet Nam

*E-mail : djajashanta@yahoo.co.id; fgulo@unsri.ac.id

ABSTRACT

The SnO₂/Sn₃O₄ were successfully prepared using a one-step hydrothermal method and exhibit the heterostructure formation. The heterostructure formation facilitates the enhancing of visible-light photoresponse of SnO₂ which well known as the UV-light activated semiconductor. The heterostructure formation also exhibits high efficient photocatalytic performance by completely degrading 10 ppm of DB71 in 120 minutes after adding 50 mg of prepared-Tin oxide with a kinetic rate constant of $4.636 \times 10^{-2} \text{ min}^{-1}$. The kinetic constant rate of prepared-Tin oxide has 2.5 and 3 times faster compared to the kinetic constant rates of SnO₂ and Sn₃O₄, respectively. The high efficient photocatalytic degradation was generated by the improvement of carrier mobilities through manipulating band alignment between SnO₂ and Sn₃O₄ and prevented the recombination of photogenerated hole-electron which commonly generated in the intrinsic semiconductor. Heterostructure SnO₂/Sn₃O₄ was not only forming high-efficiency photocatalytic degradation but also exhibiting blue shifting phenomenon. The UV-Vis adsorption response approaches were used to investigate and propose the photocatalytic degradation mechanism. After 120 minutes, there were only benzene adsorption peaks detected indicating the mineralization of DB71 dyes.

Keywords: tin oxide, hydrothermal synthesis, heterojunction, photocatalysis, degradation

© RASĀYAN. All rights reserved

INTRODUCTION

In recent decades, most of the environmental research address into developing the wastewater treatment to remove the organic pollutant which is generated by the anthropogenic activities from several sectors such as industry¹, hospital², household³, etc. Several efforts have been made and successfully remove the organic pollutants before releasing to the environment⁴⁻⁶. Although the progress on wastewater treatment has been made, most of the treatment only change the phase of a pollutant from wastewater to concentrate pollutant which further becomes the secondary pollutant due to incomplete treatment. The proper wastewater treatment is still a major challenge to find suitable wastewater treatment which could completely remove and eliminate the pollutant from wastewater.

The photocatalytic reaction had gained tremendous interest in last decades due to its potential to degrade and mineralize most of the organic pollutant through utilizing the photon energy from the light source⁷. Several semiconductors such as TiO₂, ZnO, SnO₂, and Sn₃O₄ have been successfully explored as photocatalyst and possess excellent performance in the degradation of organic pollutants⁸⁻¹⁰. Among them, Sn₃O₄ has promoted higher efficiency performance when activated by visible-light radiation ($\lambda > 390$ nm) due to its narrow band gap (~2.5 – 2.9 eV). Furthermore, the photoresponse in visible-light regions open the possibilities of Sn₃O₄ activated by sunlight irradiation as the highest visible light source in-universe. Moreover, several works have explored Sn₃O₄ as advanced material and successfully applied as chemical and gas sensors¹¹, anode materials for lithium-ion battery^{12,13}, solar cells^{14,15}, and photocatalysts¹⁶.

To be specific as photocatalytic material, the visible-light irradiation introduced the electron from valence band to conduction band of Sn₃O₄, leaving a hole (h⁺) at its surface. The photo-generated hole can oxidize the adsorbed water molecules or hydroxyl ions to produce highly oxidative agent, hydroxyl radical ($\bullet\text{OH}$), which can promote the degradation of organic molecules as contaminant¹⁷. Moreover, the narrow band gap of Sn₃O₄ has the advantageous in adsorbing the photon energy compared to the wide band gap of semiconductor because the narrow band gap can easily promote more holes using low energy wavelength (visible light wavelength)¹⁸. However, the narrow band gap semiconductor potentially has higher recombination process compared to the wide band gap semiconductor because the excited electron could easily recombine if the excited electron or hole do not spontaneously capture the target molecules. The recombination becomes the main problem in the photocatalytic reaction of narrow band gap semiconductor and should be avoided to generate high photocatalytic performance.

Currently, studying the preventing of recombination phenomenon have been successfully developed by several efforts^{19,20}. Most of the works focused on the engineering process to transfer the excited-electron to the other band of compounds to improve the lifetime of photo-generated holes which well known as the heterojunction formation. In the formation of heterojunction, the optical structure is manipulated by band alignment between two semiconductor¹⁸ resulting in high electron transfer through the interface of a junction to the opposite direction and leading to a spatial separation of photo-generated electron-hole. The effective separation suppresses the recombination process and improves the existing time of the hole, resulting in higher photocatalytic activity²¹. In addition, the manipulation of electronic structure between two semiconductors through the heterojunction formation enhance visible-light photoresponse of UV activated semiconductor²².

The formation of heterostructure has been reported by several works²³⁻²⁵ and have proved effective to enhance the photocatalytic performance²⁶. Our previous experiment²² have successfully prepared the heterostructure semiconductor of SnO₂/Sn₃O₄ by adjusting the precursor acidity which controls the phase transformation of Tin oxide²⁷. The presence of Sn₃O₄ in the heterojunction formation enhanced the visible-light photoresponse of SnO₂ which have the maximum adsorption in UV-light region. However, the enhancement of photocatalytic performance has not confirmed yet. In this study, the prepared-catalyst is tested to degrade tri-azo dye direct blue 71 which has high chemical complexity resulting in high stability. The enhancing of photocatalytic performance is confirmed by comparing the photocatalytic performance of SnO₂/Sn₃O₄ with the performance of pure SnO₂ and Sn₃O₄. Furthermore, the successful degradation of direct blue 71 could be a reference in the degradation of a high complex organic compound using high-efficiency photocatalyst.

EXPERIMENTAL

Materials

All chemicals used were analytical grade which obtained from E-Merck and was used as received without any further purification. SnCl₂.2H₂O was used as the precursor. Sodium hydroxide (NaOH) pellets were used as the precursor of a base solution to adjust the precursor initial pH. The absolute ethanol (≥ 99.5 % of purity) was used as a solvent.

Preparation of SnO₂/Sn₃O₄hetero Structure

The preparation of SnO₂/Sn₃O₄ heterostructure referred to our previous work²² with some modification. 4 mmol of SnCl₂.2H₂O (E-Merck) is well dispersed into the mixture solution of the distilled water and ethanol (2:1 v/v) and actively stirred for 30 minutes. Furthermore, the precursor acidity was adjusted to 2.5 from

pH 1 by slowly dropping 1 M NaOH. The obtained solution was carefully transferred into a Teflon-line stainless steel autoclave and hydrothermally annealed at 150°C for 12 hours with a heating rate of 50°C per minutes. The obtained-product was centrifuged at 10.000 rpm for 30 minutes and gently washed with distilled water for couple times and ethanol in the last washes. Finally, all the product was dried at 70°C for 24 hours.

Characterization

Prepared-Tin oxide was characterized using X-Ray Diffractometer (Bruker D8 Advance with Cu K α , $\lambda=0.15406$ nm) to identify the Crystal phases and composition. The surface morphology and structure of prepared-Tin oxide was imaged by Scanning Electron Microscope (Nova NanoSEM 450, FEI). The photoadsorption response in UV-and visible regions was characterized by UV-Vis spectrophotometry equipped Diffuse Reflectances Spectroscopy (Shimadzu UV-2600 Series). In order to measure the surface charge of prepared-Tin oxide, zeta potential analyzer (Malvern Zetasizer Nano Series) was employed by checking the zeta potential of prepared-Tin oxide as a function of pH.

Photocatalytic Degradation Test

50 mg of prepared-Tin oxide was suspended onto 10 ppm DB71 dye (Aldrich, 50% dye content) solution in 250 mL deionized water as an organic pollutant model. Prior to illumination, the adsorption capacity test was conducted by magnetically stirred the suspended solution (catalyst+dye) in dark condition for 30 minutes to reach adsorption-desorption equilibrium²⁸. After the adsorption capacity test, the photocatalytic test was conducted by irradiating the suspended solution with a 125 W of Mercury lamp (Osram) equipped with a cylindrical pyrex tube ($\lambda>390$ nm)²⁹. All experiments are surrounded by a circulating water jacket to cool down and stabilize the lamp temperatures and dye solutions (Figure 1). In order to evaluate the adsorption capacity and the photocatalytic performance, 7 ml of aliquots were taken every 10 and 30 minutes, respectively. All the obtained-suspended solutions from adsorption capacity and photocatalytic tests were centrifuged and decanted to remove catalyst powder. Discoloration performance was well-controlled at a maximum wavelength of DB71 at 588 nm by UV-Vis spectrophotometer (Philips US5300). Effect of light irradiation to dyes degradation was also studied through photolysis experiment by irradiating DB71 dyes with the absence of catalyst³⁰.

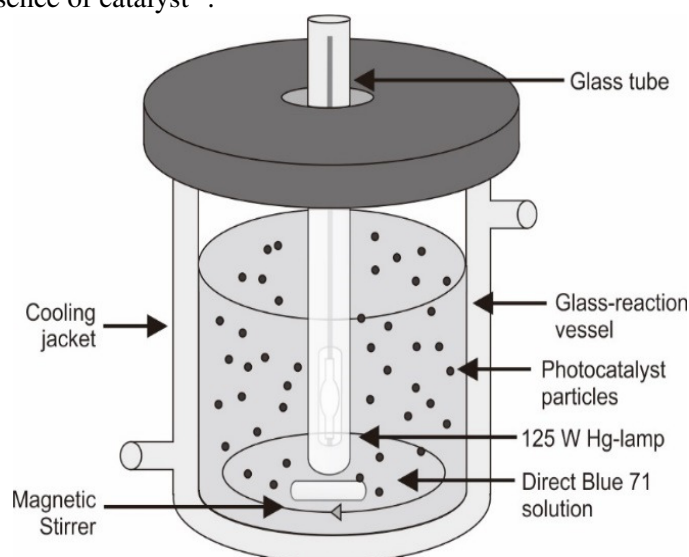


Fig.-1: Photocatalytic Reactor Design

RESULTS AND DISCUSSION

Characterization Results

Figure-2 showed that prepared-Tin oxide exhibited two sharp diffraction peaks of a mixture between tetragonal SnO₂ (JCPDS No. 1445) and triclinic Sn₃O₄ (JCPDS No. 16. 0737). There is no SnO or other

mixed-valent Tin oxide diffractions was observed in all diffractions, indicating that only SnO_2 and Sn_3O_4 phases generated during the preparation process.

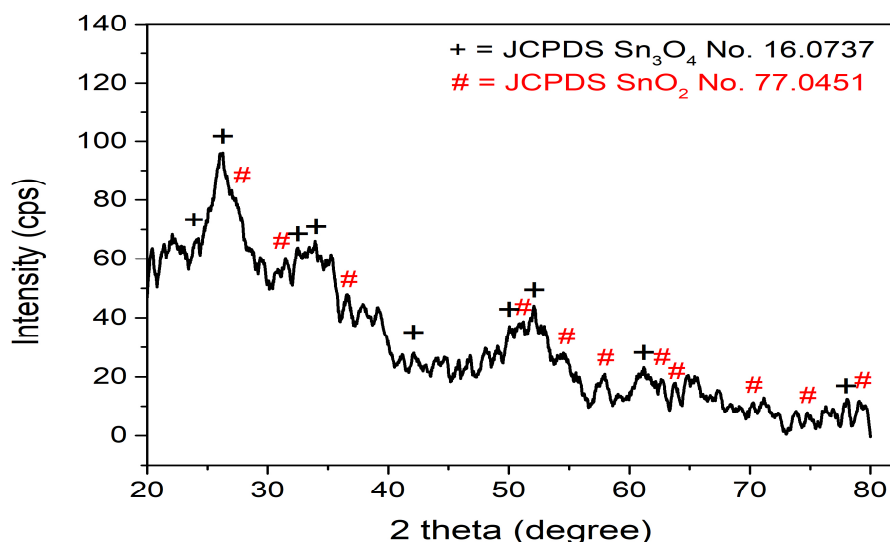


Fig.-2: The Peak of XRD Patterns of prepared-Tin Oxide. + = Sn_3O_4 and # = SnO_2

The results of the scanning electron microscope in Fig.-3 clearly showed that $\text{SnO}_2/\text{Sn}_3\text{O}_4$ have flower-like nanostructure with prickly sheets shape in detail^{27,31}. Furthermore, most of the prepared-Tin oxide surface had rough surface generated by the high formation of agglomeration, indicating prepared-Tin oxide consists of many small particles (in nano-sized).

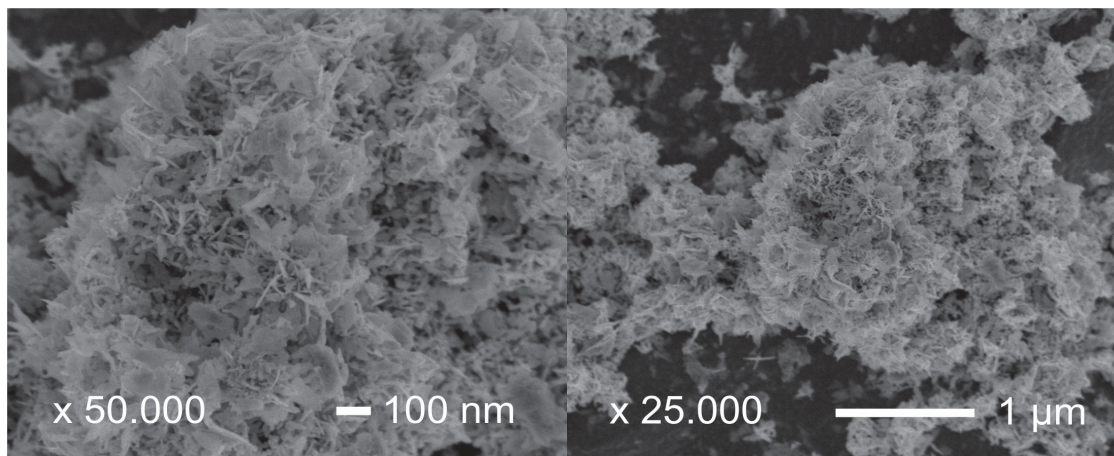


Fig.-1: Scanning Electron Microscopy Images of prepared-Tin Oxide with Different Magnification.

The photoresponses properties of prepared-Tin oxide clearly exhibited visible-light photoresponse (Fig.-4), suggesting that prepared-Tin oxide has a narrow band gap semiconductor corresponding to the energy band gap of Sn_3O_4 ³². The presence of Sn_3O_4 in $\text{SnO}_2/\text{Sn}_3\text{O}_4$ heterostructure provides the contribution in enhancing visible-light photoresponse of SnO_2 which activate in UV-light region. To gain insight into the photoresponses properties of Tin oxides, Tauc equation was employed to calculate the bandgap energy of $\text{SnO}_2/\text{Sn}_3\text{O}_4$ ³³.

The band gap energy is determined by calculating the slope by plotting $(\alpha h\nu)^n$ versus photon energy in electron volt (eV). Inset image in Fig.-4 clearly shows the formation of heterostructure $\text{SnO}_2/\text{Sn}_3\text{O}_4$ confirmed by two slopes of band gap energy.

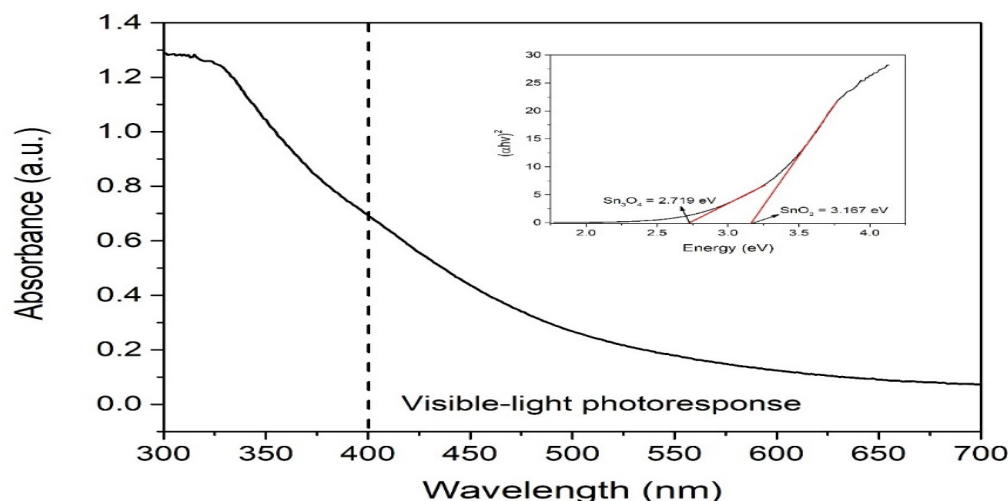


Fig.-2: UV-Visible Absorption Spectra of prepared-Tin Oxides

From utilizing the Tauc equation, the calculated-bandgap of SnO_2 and Sn_3O_4 consisted of heterostructure $\text{SnO}_2/\text{Sn}_3\text{O}_4$ are 3.167 eV and 2.719 eV, respectively. The formation of type I heterostructure $\text{SnO}_2/\text{Sn}_3\text{O}_4$ is in accordance with the work reported by Xia (2014)²⁶. Furthermore, the calculated-band gap was used to calculate the minimum wavelength to activate the catalyst during the photocatalytic test by employing the eqn.-1. The calculation results 391 nm and 456 nm as minimum energy to activate SnO_2 and Sn_3O_4 , respectively. Therefore, in this experiment, we used 125W of Hg-lamp equipped with a glass tube to ensure that all the light irradiate the proper photon energy because of subjected by UVA and Visible wavelength ($\lambda > 390$ nm).

$$E \text{ (eV)} = \frac{1240}{\lambda \text{ (nm)}} \quad (1)$$

Before measuring the photocatalytic performance of $\text{SnO}_2/\text{Sn}_3\text{O}_4$, the preliminary control tests are performed through measuring adsorption capacity of $\text{SnO}_2/\text{Sn}_3\text{O}_4$ by directly mixing prepared-Tin oxide with dyes in dark condition. The result in Fig.-5 demonstrated that $\text{SnO}_2/\text{Sn}_3\text{O}_4$ have low adsorption capacities by only removing approximately 1.4 % of color after 30 minutes of contact time. The low adsorption capacities are generated by the high formation of agglomeration in the powder system during the photocatalytic test. In addition, the low adsorption capacities are generated by electrostatic repulsion between sample dyes and surface of the catalyst. Zeta potential measurement shows that $\text{SnO}_2/\text{Sn}_3\text{O}_4$ have negative charges at pH 5 (the natural pH of DB71) with pH_{zpc} around 3 (Inset image in Fig.-5). Meanwhile, there will be an electronic repulsion between negative charges of catalyst surface and the functional group of dyes which is categorized as negatively charged of a sulphonic group of DB71 resulting in low adsorption capacities³⁴. However, it is postulated that small amount of removal through the adsorption process is performed by weak electrostatic interaction between positively charged of the tri-azo group and negative charges of Tin oxide surfaces. Furthermore, we propose the possible mechanism of electrostatic interaction and repulsion of DB71 with surface charge of prepared-Tin oxide in Fig.-6.

The photocatalytic activities of prepared-Tin oxide were evaluated by degrading tri-azo direct blue 71 (DB71) dyes under UV-visible irradiation. The pure SnO_2 (Sigma Aldrich, 99.9% of purity) and the single phase of triclinic Sn_3O_4 were also tested to compare their performance with prepared $\text{SnO}_2/\text{Sn}_3\text{O}_4$. Fig.-7 clearly reveals that photodegradation of DB71 in the presence of 50 mg $\text{SnO}_2/\text{Sn}_3\text{O}_4$ semiconductor performs the most efficient degradation of DB71 than the photocatalytic activities of pure SnO_2 and Sn_3O_4 . The high photocatalytic activities of $\text{SnO}_2/\text{Sn}_3\text{O}_4$ are generated by the formation of type I heterostructure which prevents recombination of photogenerated hole-electron and improves the electronic and optical properties by driving carrier mobilities¹⁸. To be specific, the formation of heterostructure facilitates electron transfer from valence bands of both SnO_2 and Sn_3O_4 to the conduction band of Sn_3O_4 which are continuously injected to the conduction band of SnO_2 . Thus, the more photogenerated electrons accumulated in the conduction band of SnO_2 generates more photogenerated holes in the valence band of SnO_2 showing the

effective spatial separation which increases the lifespan of photogenerated electrons-holes. This condition generates higher photocatalytic performance compared to the intrinsic semiconductor which only has direct excitation pathways from the valence band to conduction band. Furthermore, the direct excitation pathway easily recombines the excited electron and hole, resulting in lower photocatalytic performance. In this study, the plentiful amount of photon energy effectively excites an electron from the conduction band of SnO_2 and Sn_3O_4 which is reported having high adsorption performance in UV wavelength.

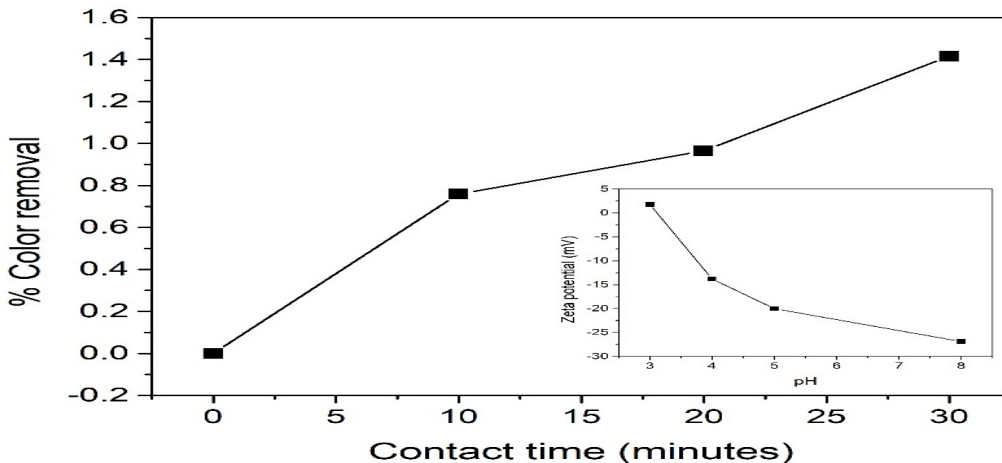


Fig.-3: Adsorption Capacity of prepared-Tin Oxide in DB71 Color Removal. Inset Image is the Data of Zeta Potential Measurement as a Function of pH Solution.

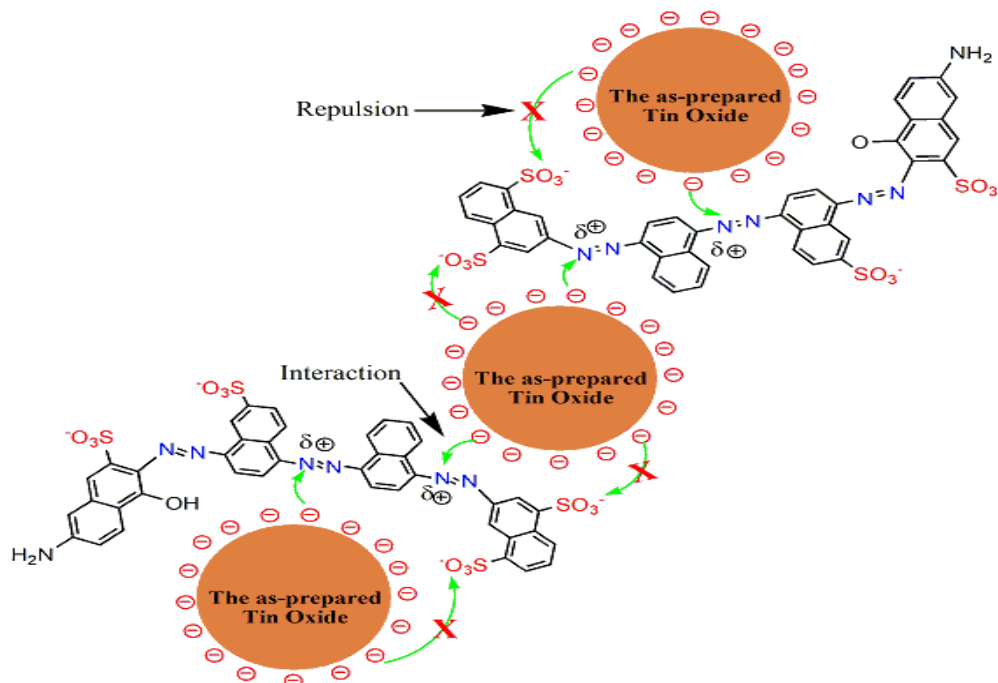


Fig.-6: Proposed-Electrostatic Interaction/Repulsion Between prepared-Tin Oxide and Anionic Functional Group of Direct Blue 71 (DB71) Dyes

The kinetic rate calculation is further used to investigate the enhancement of photocatalytic performance. All obtained data is fitted with the pseudo-first-order kinetics model which was employed by plotting $-\ln(C_t/C_0)$ obtained from discoloration of DB71 dyes as a function of light irradiation time by following the eqn.-2:

$$-\ln\left(\frac{C_t}{C_0}\right) = kt \tag{2}$$

Where, C_t and k (min^{-1}) are the concentration of DB71 at a specific time and the photocatalytic degradation rate constant, respectively.

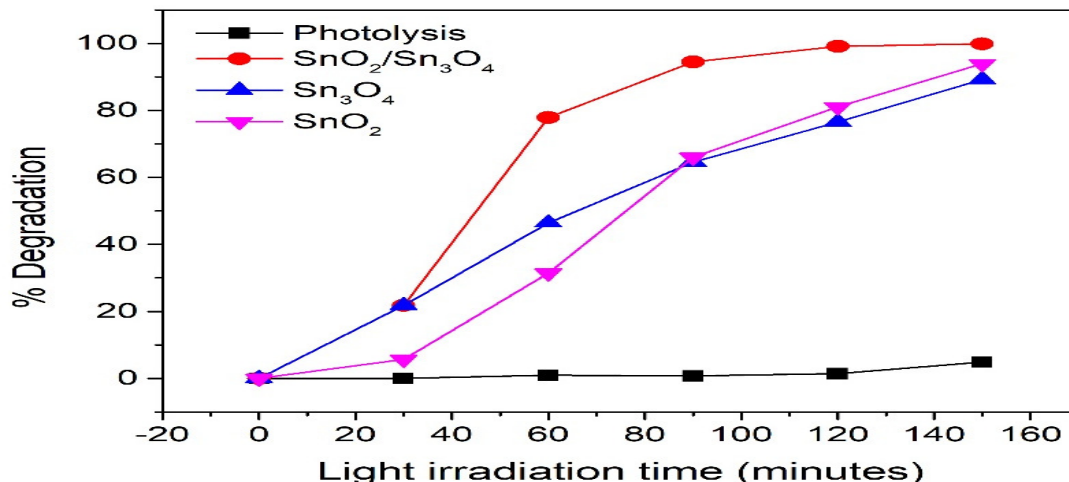


Fig.-7: Percentages of DB71 Color Removal through Degradation Over the Photolysis and Photocatalysis Tests

The photocatalytic degradation rate of SnO₂/Sn₃O₄ has $4.636 \times 10^{-2} \text{ min}^{-1}$ which is 2.5 and 3 times faster compared to SnO₂ ($1.859 \times 10^{-2} \text{ min}^{-1}$) and Sn₃O₄ ($1.444 \times 10^{-2} \text{ min}^{-1}$), respectively. The linear relationships between $-\ln(C/C_0)$ and the light irradiation time are well found in fitting with more than 90% linear fit of adjusted R square (R^2) except the photocatalytic degradation conducted by SnO₂ (89%) indicating the excellent agreement with the pseudo-first-order kinetics model.

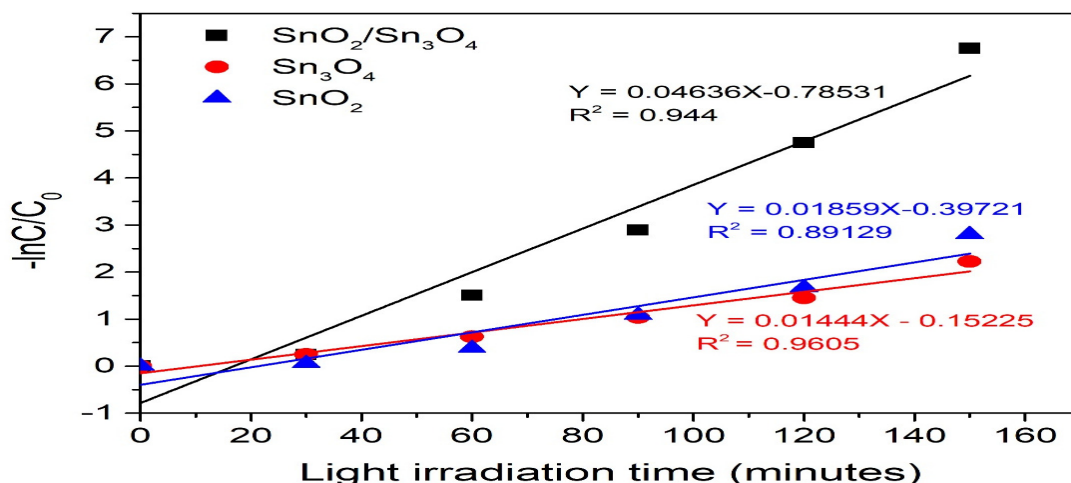
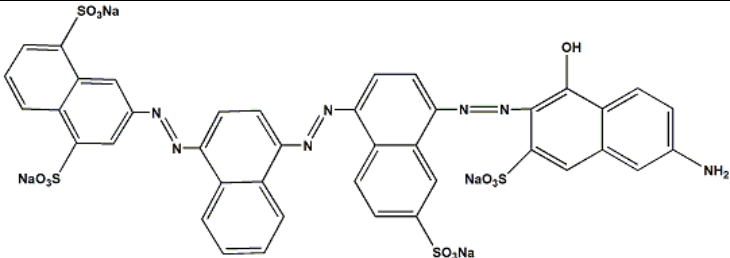
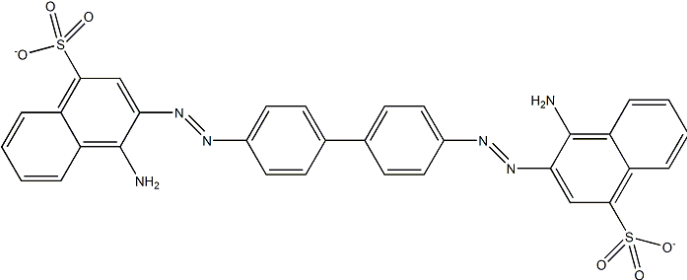
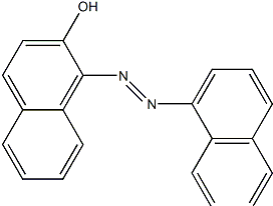
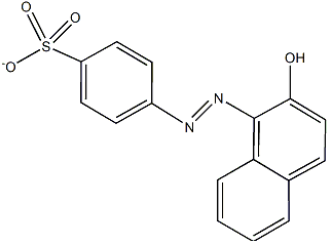
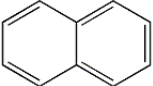
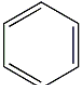


Fig.-8: Curve of Kinetic Rate Constants of DB71 Degradation using prepared-Tin Oxide, Pure SnO₂, and Sn₃O₄. Insert Equations showed Linear Regression Lines and Adjusted R Square.

Moreover, not only forming high-efficiency photocatalytic degradation, prepared-Tin oxide exhibited three times of blue shifting phenomenon during photocatalytic degradation (Figure 9). In literature reviews³⁵⁻³⁷, blue shifting phenomenon is originated from de-ethylation and/or de-methylation process of dyes through the mineralization process resulting in the formation of intermediate phases. In order to propose the intermediate phases and photocatalytic degradation mechanism, the investigation is done by investigating maximum adsorption wavelength changes of dyes after treatment. The shifting of maximum wavelength is

correlated by changing the chemical structure of dye. In order to see how the chemical structure changes the maximum wavelength, we tried to trace the sub-class and derivatives of DB71 which potential become the intermediate phase of DB71 and matched their structure with their maximum wavelength. Table-1 presents some sub-class and derivatives of azo dyes which have a similar structure with the functional group of DB71. This approach is also done by investigating the correlation between the maximum wavelength and the chemical structure of dyes.

Table-1: Adsorption Peak of Several Dyes as the Comparison Standard in Determining the Intermediate Compounds appeared during Photocatalytic Degradation of DB71

Compounds	Structure	Absorption Peak (nm)
Direct Blue 71		588
Direct Red 28		500
Acid Red 88		505
Acid Orange 7		542
Naphthalene		286
Benzene		255

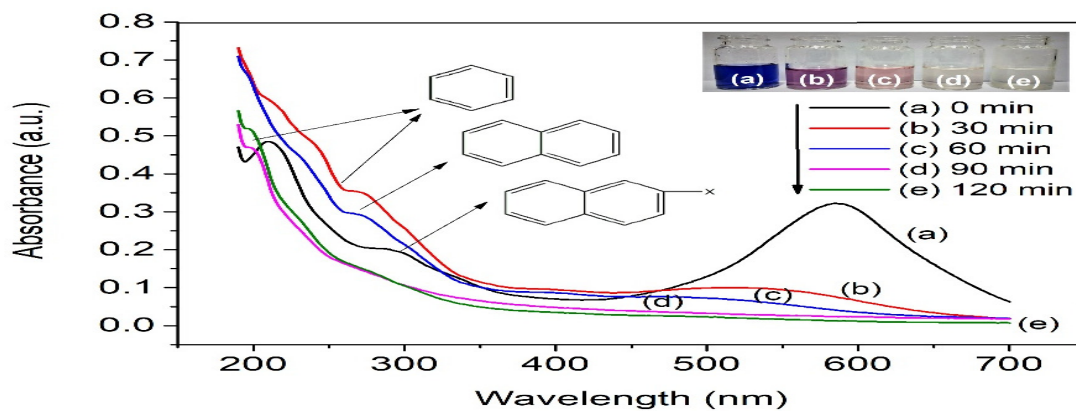


Fig.-9: Photo-response of treated-DB71 using the prepared-Tin Oxide. Inset Image shows Color Gradation due to the blue Shifting Phenomenon

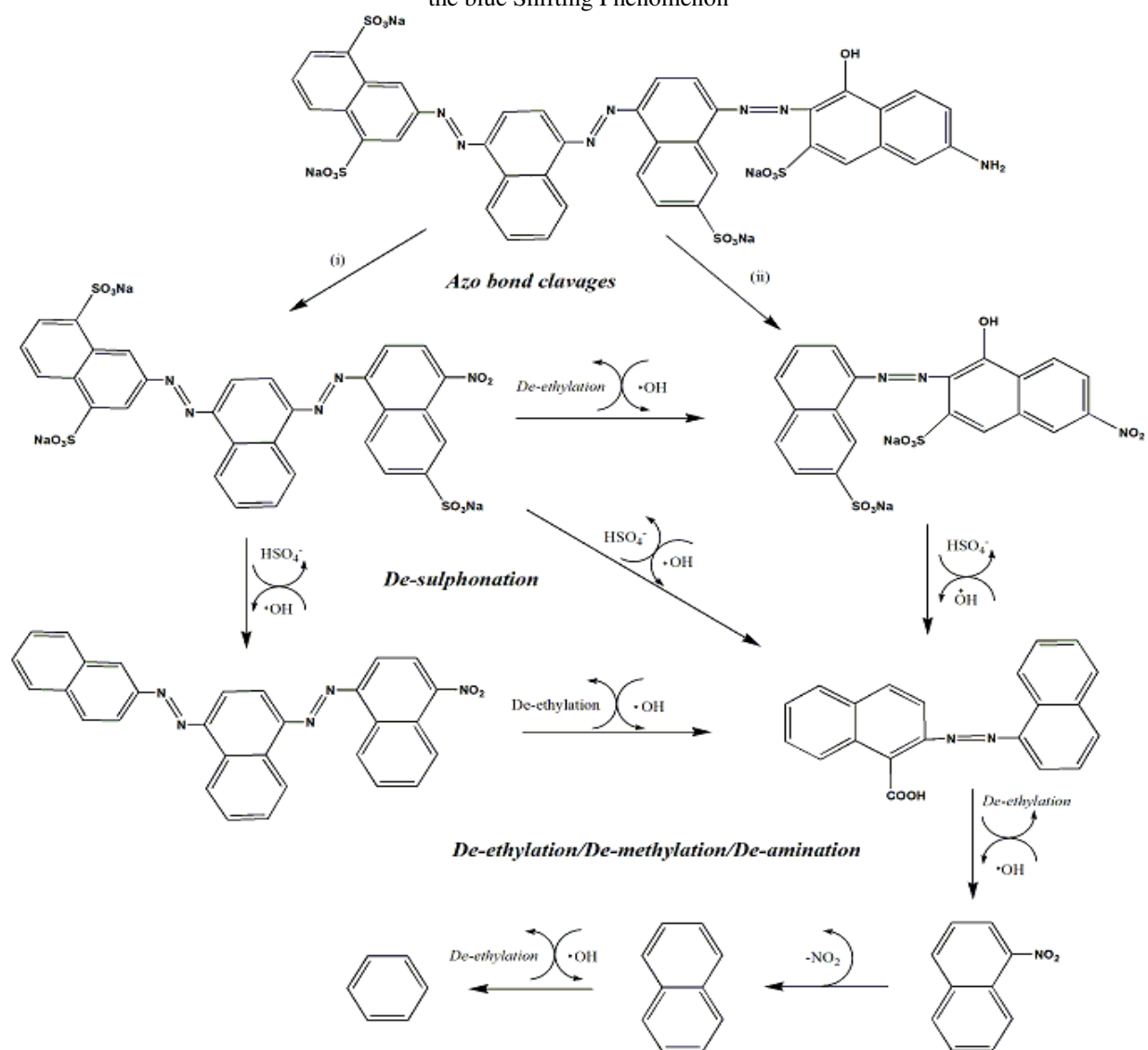


Fig.-10: Proposed-pathways of Photocatalytic Degradation of DB71 using prepared-Tin Oxide

After investigating the correlation between the chemical structure of sub-class and derivatives of DB71, the photocatalytic degradation mechanism is proposed. According to our analysis, the photocatalytic degradation mechanism is begun by attacking azo linkage of DB71 marked as the adsorption band responses

in a visible light region located at ~580 nm owing to $n \rightarrow \pi^*$ transition. Furthermore, the breakage of azo linkage continues and forms the red colored dye solution which has naphthalene functional group as chromophore detected in 285 nm of wavelength and it has 500-530 nm as maximum adsorption spectrum³⁸. It could be proposed that this is the first intermediate product which has a chemical structure like Acid Red 88 (Table-1). Moreover, photocatalytic degradation is regularly continued by degrading another chromophore group through N-demethylation, de-amination and oxidative degradation leaving benzene and naphthalene rings which relatively having no color but clearly detected in peaks UV-vis spectrophotometer (Fig.-9)^{38,39}. However, some peaks in UV wavelength is still detected after 120 min of light irradiation such as benzene and naphthalene due to the formation of some intermediate of aromatic rings. Figure-10 shows proposed-photocatalytic mechanism using prepared-Tin oxide.

CONCLUSION

The high efficient visible-light activated photocatalytic semiconductor have successfully synthesized using the one-step hydrothermal method and form type I heterostructure SnO₂/Sn₃O₄. The photocatalytic test shows that SnO₂/Sn₃O₄ has high-efficient photocatalytic degradation of DB71 with a kinetic rate constant of $4.636 \times 10^{-2} \text{ min}^{-1}$ which is 2.5 and 3 times faster compared to SnO₂ ($1.859 \times 10^{-2} \text{ min}^{-1}$) and Sn₃O₄ ($1.444 \times 10^{-2} \text{ min}^{-1}$), respectively. The study proved that heterostructure formation of tin oxides prevents the recombination of photogenerated hole-electron which commonly generated in intrinsic semiconductor and improves the electronic and optical properties by driving carrier mobilities. We believe that SnO₂/Sn₃O₄ has the potential to become a high-efficiency photocatalytic semiconductor which offers an energy-saving option for removal treatment of environmental pollutants.

ACKNOWLEDGMENT

The authors acknowledge the Ministry of Research, Technology, and Higher Education of the Republic of Indonesia who provides the scholarship and research funding through PMDSU Batch II Program. The authors also thank the Rohan Project funded by the German Academic Exchange Service (DAAD, No. 57315854) and the Federal Ministry for Economic Cooperation and Development (BMZ) inside the framework "SDG Bilateral Graduate School Program" for supporting the collaborative research between Universitas Sriwijaya and Hanoi University of Science, Vietnam National University.

REFERENCES

1. A. Ashok, K. Raman, S.A. Masilamani, R.S.C. Bose, *Rasayan J Chem.*, **11(1)**, 53(2018), DOI:10.7324/RJC.2018.1111969.
2. I. Kurniawan, S. Nasir, M. Hermansyah, *Pollut Res Pap.*, **36(2)**, 343(2017).
3. A. Ghawi, *J Ecol Eng.*, **19(2)**, 63 (2018), DOI:10.12911/22998993/81780.
4. M. Vakili, M. Rafatullah, B. Salamatinia, A.Z. Abdullah, M.H. Ibrahim, K.B. Tan, Z. Gholami, P. Amouzgar, *Carbohydr Polym.*, **113**, 115(2014), DOI:10.1016/j.carbpol.2014.07.007.
5. J. Mateo-Sagasta, L. Raschid-Sally, A. Thebo, Global Wastewater and Sludge Production, Treatment and Use. In: *Wastewater*. Dordrecht: Springer Netherlands, 15-38 (2015), DOI:10.1007/978-94-017-9545-6_2.
6. C.T. Handoko, A. Huda, M.D. Bustan, B. Yudono, F. Gulo, *Rasayan J Chem.*, **10(4)**, 1137(2017), DOI:10.7324/RJC.2017.1041875.
7. D.I. Prajapati, H.S. Sharma, R. Ameta, *Rasayan J Chem.*, **11(3)**, 1311(2018), DOI:10.31788/RJC.2018.1132071.
8. A. Hernández-Ramírez, I. Medina-Ramírez, eds. *Photocatalytic Semiconductors*. Cham: Springer International Publishing, 1-5 (2015), DOI:10.1007/978-3-319-10999-2.
9. K. Nakata, A. Fujishima, *J Photochem Photobiol C Photochem Rev.*, **13(3)**, 169(2012), DOI:10.1016/j.jphotochemrev.2012.06.001.
10. M.T. Uddin, Y. Nicolas, C. Olivier, T. Toupance, L. Servant, M.M. Müller, H.-J. Kleebe, J. Ziegler, W. Jaegermann, *Inorg Chem.*, **51(14)**, 7764(2012), DOI:10.1021/ic300794j.
11. X. Li, F. Wang, J. Tu, H.U. Shah, J. Hu, Y. Li, Y. Lu, M. Xu, *J Nanomater.*, **2015**, 1(2015), DOI:10.1155/2015/980170.
12. J. Li, Y. Zhao, N. Wang, L. Guan, *Chem Commun (Camb.)*, **47(18)**, 5238(2011),

- DOI:10.1039/c1cc10542f.
13. S.-L. Yang, B.-H. Zhou, M. Lei, L.-P. Huang, J. Pan, W. Wu, H.-B. Zhang, *Chinese Chem Lett.*, **26(10)**, 1293(2015), DOI:10.1016/j.ccllet.2015.05.051.
 14. R. Vasanthapriya, N. Neelakandeswari, N. Rajasekaran, K. Uthayarani, M. Chitra, S.K. Sathiesh, *Mater Lett.*, **220**, 218(2018), DOI:10.1016/j.matlet.2018.02.118.
 15. I.Y.-Y. Bu, *Opt - Int J Light Electron Opt.*, **147**, 39(2017), DOI:10.1016/j.ijleo.2017.08.061.
 16. Y. He, D. Li, J. Chen, Y. Shao, J. Xian, X. Zheng, P. Wang, *RSC Adv.*, **4**, 1266(2014), DOI:10.1039/C3RA45743E.
 17. A. Ajmal, I. Majeed, R.N. Malik, H. Idriss, M.A. Nadeem, *RSC Adv.*, **4**, 37003(2014), DOI:10.1039/C4RA06658H.
 18. H. Pan, *Renew Sust Energ Rev.*, **57**, 584(2016), DOI:10.1016/j.rser.2015.12.117.
 19. G.G. Bessegato, J.C. Cardoso, M.V.B. Zanoni, *Catal Today*, **240**, 100(2015), DOI:10.1016/j.cattod.2014.03.073.
 20. M. Raza, Z. Kanwal, A. Rauf, A. Sabri, S. Riaz, S. Naseem, *Nanomaterials*, **6(4)**, 74(2016), DOI:10.3390/nano6040074.
 21. W. Fan, Q. Zhang, Y. Wang, *Phys Chem Chem Phys.*, **15**, 2632(2013), DOI:10.1039/c2cp43524a.
 22. A. Huda, R. Ichwani, C.T. Handoko, B. Yudono, M.D. Bustan, F. Gulo, *Mater Lett.*, **238**, 264 (2019), DOI:10.1016/j.matlet.2018.11.169.
 23. Y. Wang, Q. Wang, X. Zhan, F. Wang, M. Safdar, J. He, *Nanoscale*, **5**, 8326(2013), DOI:10.1039/c3nr01577g.
 24. D. Sarkar, C.K. Ghosh, S. Mukherjee, K.K. Chattopadhyay, *ACS Appl Mater Interfaces*, **5(2)**, 331(2013), DOI:10.1021/am302136y.
 25. Z. Liu, D.D. Sun, P. Guo, J.O. Leckie, *Nano Lett.*, **7(4)**, 1081(2007), DOI:10.1021/nl061898e.
 26. W. Xia, H. Wang, X. Zeng, J. Han, J. Zhu, M. Zhou, S. Wu, *CrystEngComm.*, **16**, 6841(2014), DOI:10.1039/C4CE00884G.
 27. A. Huda, C.T. Handoko, M.D. Bustan, B. Yudono, F. Gulo, *Mater Lett.*, **211**, 293(2018), DOI:10.1016/j.matlet.2017.10.029.
 28. D.D. Mishra, Y. Huang, N. Duan, G. Tan, *J Mater Sci Mater Electron*, **29(12)**, 9854(2018), DOI:10.1007/s10854-018-9025-0.
 29. C.W. Dunnill, *Int J Photoenergy*, **2014**, 407027(2014), DOI:10.1155/2014/407027.
 30. B. Huang, J. He, S. Bian, C. Zhou, Z. Li, F. Xi, J. Liu, X. Dong, *Chinese Chem Lett.*, **29(11)**, 1698(2018), DOI:10.1016/j.ccllet.2018.01.004.
 31. X. Chen, Y. Huang, T. Li, C. Wei, J. Yan, X. Feng, *Appl Surf Sci.*, **405**, 13(2017), DOI:10.1016/j.apsusc.2017.01.244.
 32. M. Manikandan, T. Tanabe, P. Li, S. Ueda, G.V. Ramesh, R. Kodiyath, J. Wang, T. Hara, A. Dakshanamoorthy, S. Ishihara, K. Ariga, J. Ye, N. Umezawa, H. Abe, *ACS Appl Mater Inter.*, **6(6)**, 3790(2014), DOI:10.1021/am500157u.
 33. D. Leng, L. Wu, H. Jiang, Y. Zhao, J. Zhang, W. Li, L. Feng, *Int J Photoenergy*, **2012**, 235971(2012), DOI:10.1155/2012/235971.
 34. M. Wawrzekiewicz, M. Wiśniewska, V.M. Gun'ko, V.I. Zarko, *Powder Technol.*, **278**, 306(2015), DOI:10.1016/j.powtec.2015.03.035.
 35. W. Szeto, C.W. Kan, C.W.M. Yuen, S-W. Chan, K.H. Lam, *Int J Chem Eng.*, **2014**, 270946(2014), DOI:10.1155/2014/270946.
 36. C. Chen, C. Lu, *J Phys Chem C.*, **111**, 13922(2007), DOI:10.1021/jp0738964.
 37. M. Rochkind, S. Pasternak, Y. Paz, *Molecules*, **20(1)**, 88(2014), DOI:10.3390/molecules20010088.
 38. D. Li, L. Qian, Y. Feng, J. Feng, P. Tang, L. Yang, *ACS Appl Mater Interfaces*, **6(23)**, 20603(2014), DOI:10.1021/am506696k.
 39. K. Dai, H. Chen, T. Peng, D. Ke, H. Yi, *Chemosphere*, **69(9)**, 1361(2007), DOI:10.1016/j.chemosphere.2007.05.021.

[RJC-5084/2013]